ACS Partner Journal
PRECISION CHEMISTRY

Cryogenic Photodetachment Spectroscopy and High-Resolution Resonant Photoelectron Imaging of Cold *para*-Ethylphenolate Anions

Dao-Fu Yuan, Yue-Rou Zhang, Chen-Hui Qian, Guo-Zhu Zhu, and Lai-Sheng Wang*

Cite This: *Precis. Chem.* 2023, 1, 161−174 **Read Online**

ACCESS | Metrics & More | Article Recommendations | Supporting Information

ABSTRACT: Valence-bound molecular anions with polar neutral cores (μ > 2.5 D) can support highly diffuse dipole-bound states (DBSs) as electronically excited states just below the detachment threshold. Such weakly bound nonvalence excited states have little influence on the structure of the neutral core, and they usually have the same vibrational frequencies. DBSs can be systematically searched using photodetachment spectroscopy (PDS), which can yield the binding energies of the DBSs, the electron detachment threshold of the anion, and above-threshold vibrational levels of the DBSs (Feshbach resonances). We have shown that the combination of PDS and resonant photoelectron spectroscopy (rPES) at the Feshbach resonances is a powerful approach to obtain rich vibrational information for complex molecular radicals. A prerequisite for this technique is to produce vibrationally cold anions, made possible by a cryogenically controlled Paul trap. In this article, we report a PDS and rPES study of cold *para*-ethylphenolate anions (*p*-EP⁻). The electron affinity of the *p*-EP radical is measured to be 17425 ± 3 cm^{-1} (2.1604 ± 0.0004 eV), and a DBS is found at 145 cm^{-1} below the detachment threshold of *p*-EP⁻. Thirty-four vibrational levels are observed for the DBS, including two bound levels and 32 Feshbach resonances. Frequencies for 17 vibrational modes of the *p*-EP radical are measured from the combination of PDS and rPES, including six symmetry-forbidden modes with A″ symmetry. The current study confirms again the power of combining cryogenic ion cooling with PDS and high-resolution rPES to obtain spectroscopic information on complex molecular radicals.

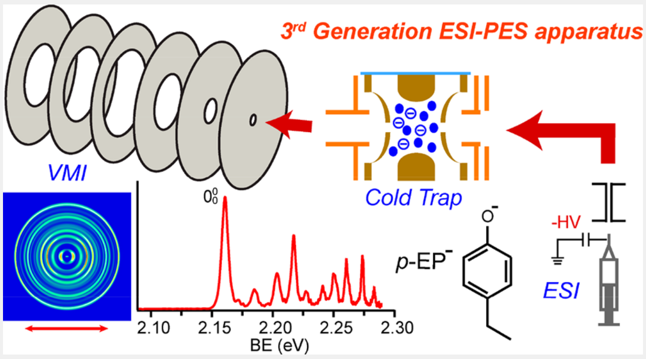

KEYWORDS: *dipole-bound state, photoelectron imaging, cryogenic ion cooling, resonant photoelectron spectroscopy, ethylphenoxy radical, vibrational frequencies, electrospray ionization*

1. INTRODUCTION

Photoelectron spectroscopy (PES) of negative ions is one of the most powerful techniques to probe the electronic structure and chemical bonding of size-selected clusters.[1,2] The energy resolution of PES with time-of-flight (TOF) and hemispherical electrostatic energy analyzers are usually limited to several meV. High-resolution photoelectron imaging (PEI) of negative ions using slow electron velocity map imaging has allowed sub-meV energy resolution with angular distributions.[3] Aside from photoelectron energy resolution of a given PES technique, rovibrational hot bands of anions are the bottleneck for high-resouation PES, especially for large molecular systems with rich low-frequency modes. Therefore, ion cooling is essential for high-resolution PES.[4,5] On the other hand, vibrational excitations in conventional PES are governed by the Franck-Condon (FC) principle, and usually only a few symmetry-allowed vibrational modes are active and observable. Thus, despite the potential of PES to yield spectroscopic information for the neutral final states, it is not possible to observe FC-inactive vibrational modes, especially low-frequency modes for complex molecular species, which contain important fingerprint information on the overall molecular structures, but are challenging to obtain even for infrared spectroscopy. Over the past several years, we have shown that the combination of photodetachment spectroscopy (PDS) and resonant PES (rPES) via dipole-bound states (DBSs) of cryogenically cooled anions is a promising technique to obtain rich vibrational information for polar neutral species,[6] not possible in conventional PES.

Polar neutral molecules with a sufficiently large dipole moment could form dipole-bound anions by binding an excess electron via long-range charge-dipole interactions.[7−10] Va-

Received: December 24, 2022
Revised: January 18, 2023
Accepted: February 1, 2023
Published: February 15, 2023

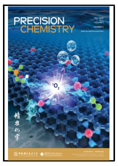

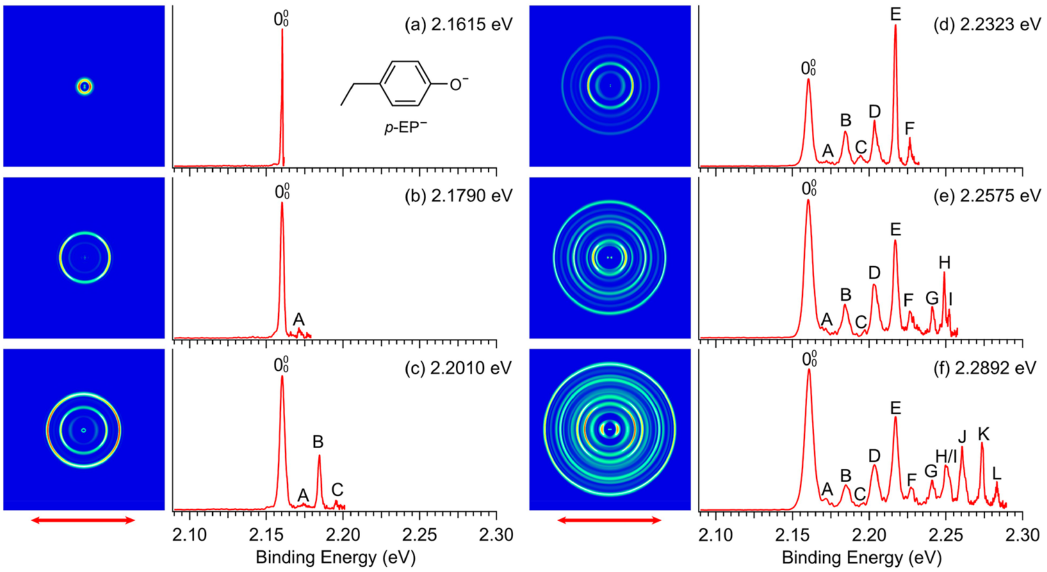

Figure 1. Photoelectron images and spectra of *p*-EP$^-$ at (a) 2.1615 eV (17434 cm^{-1}) (inset: the structure of *p*-EP$^-$), (b) 2.1790 eV (17575 cm^{-1}), (c) 2.2010 eV (17752 cm^{-1}), (d) 2.2323 eV (18005 cm^{-1}), (e) 2.2575 eV (18208 cm^{-1}), and (f) 2.2892 eV (18464 cm^{-1}). The double arrow below the images indicates the direction of the laser polarization.

lence-bound anions with a polar neutral core can have diffuse dipole-bound states as a special class of excited electronic states just below the electron detachment threshold,[11−20] analogous to Rydberg states of neutral molecules. The critical dipole moment to support dipole-bound anions was experimentally determined to be around 2.5 D,[21−23] and it was reaffirmed in a PDS and rPES study of a series of valence-bound *para*-halogen-substituted phenoxide anions (*p*-$XC_6H_4O^-$, X = F, Cl, Br, and I),[24] which have similar molecular structures and polarizability but variable dipole moments. Since the diffuse dipole-bound electron has little effect on the structure of the neutral core, dipole-bound anions and the corresponding neutral species have parallel potential energy surfaces and identical vibrational frequencies. Therefore, excitations to Feshbach resonances can autodetach to specific vibrational levels of the neutral by coupling vibrational energies to the dipole-bound electron with a propensity rule of $\Delta v = -1$.[25,26] DBSs in valence-bound anions can be searched systematically using PDS by measuring the total detachment cross section as a function of photon energy. PDS of dipole-bound anions usually exhibits similar vibrational features as conventional PES but has higher sensitivity and spectral resolution, which can provide additional vibrational information on the neutral species.[6] In particular, resonant PES at the Feshbach resonances produces a completely non-Franck-Condon vibrational profile, often lighting up vibrational final states with low FC factors or entirely new vibrational states not observable in conventional PES.[27−49] All these advances are made possible by the enabling technology of active anion cooling in a cryogenically controlled 3D Paul trap coupled with an electrospray ionization (ESI) ion source.[4]

We have developed the third-generation ESI-PES apparatus[50] coupling high-resolution photoelectron imaging (PEI),[51] cryogenic ion cooling in a 3D Paul trap, and tunable detachment laser, following the first generation ESI-PES apparatus with a room temperature Paul trap and a magnetic-bottle photoelectron analyzer[52] and the second generation ESI-PES featuring a cryogenically controlled Paul trap and a magnetic-bottle photoelectron analyzer.[4] While the best resolution on the magnetic-bottle analyzer was 11 meV, we can achieve a photoelectron energy resolution of 1.2 cm^{-1} (0.15 meV) with an optimized multilens velocity map imaging (VMI) system.[51] With the complete elimination of vibrational hot bands, the third-generation ESI-PES apparatus has allowed us to develop rPES using Feshbach resonances of DBSs as the intermediate states and to investigate a wide variety of cryogenically cooled anions.[27−49] The vibrational information obtained for neutral radicals in our study often rivals infrared spectroscopy. In addition, rich photophysical processes involving intramolecular relaxation from DBSs have been observed from rPES.[38,44] Single-color resonant two-photon detachment (R2PD) PES has allowed us to probe the nature of the DBS.[40,41,43] In rare cases, intramolecular inelastic rescattering between the outgoing autodetached dipole-bound electron and the neutral molecular core has been observed, analogous to electron energy loss spectroscopy.[35]

In the current article for the inaugural issue of *Precision Chemistry*, we report a PDS and rPES study of cryogenically cooled *p*-ethylphenolate anion (*p*-EP$^-$; see the inset of Figure 1a for its structure). The *para*-alkyl-substituted phenol is the chromophore of the amino acid tyrosine.[53] These molecules are important models for interpreting the spectrum and photochemical behaviors of tyrosine. The *p*-EP neutral has a dipole moment of 4.85 D, which is much larger than the critical value for the formation of DBS. Indeed, a DBS was observed in a previous low-resolution PDS study using room temperature anions.[54] However, no spectral information was obtained, and even the electron affinity (EA) of *p*-EP was not measured because of the low spectral resolution and extensive vibrational hot bands. The presence of the ethyl group makes the spectroscopy of *p*-EP much more complicated due to its low symmetry (C_s) and low-frequency vibrational modes. Thus, it is an excellent system to test the capability of our third-generation ESI-PES apparatus. Our previous study suggested that the intramolecular inelastic rescattering appeared to excite low-frequency (large amplitude) vibrational modes.[35] Thus, we are interested in examining the possibility of intramolecular inelastic recattering in the rPES of *p*-EP$^-$

because the lowest-frequency mode of *p*-EP (ν_{48}, A″ symmetry, Figure S1) has a frequency of only 36 cm^{-1}.

We are able to accurately measure the EA of *p*-EP as 2.1604 ± 0.0004 eV (17425 ± 3 cm^{-1}). PDS reveals a DBS at 0.0180 ± 0.0004 eV (145 ± 3 cm^{-1}) below the detachment threshold, as well as a bound vibrational level at 61 cm^{-1} below the detachment threshold. Thirty-two Feshbach resonances are observed in an energy range about 1220 cm^{-1} above the zero-point level of the DBS. The combination of PDS and rPES leads to the measurement of vibrational frequencies for 17 vibrational modes of *p*-EP, including the two lowest-frequency modes, 34 cm^{-1} for the ν_{48} (A″) mode and 89 cm^{-1} for the ν_{27} (A′) mode. Intramolecular inelastic rescattering between the outgoing autodetached electron and the molecular core is observed. The current work demonstrates again the power of PDS and rPES of cold anions to obtain rich spectroscopic information for complex molecular radicals with low-frequency vibrational modes.

2. EXPERIMENTAL AND COMPUTATIONAL METHODS

The experiment was carried out using our third-generation ESI-PES apparatus[50] equipped with a cryogenically cooled 3D Paul trap[4] and a high-resolution VMI system.[51] The *p*-EP$^-$ anion was produced by electrospray of a 1 mM solution of *p*-ethylphenol (Sigma-Aldrich, 99%) in a mixed solvent of CH_3OH/H_2O (9/1 ratio in volume) tuned to pH ~10 with NaOH to enhance deprotonation. The *p*-EP$^-$ anions generated in the ESI source were guided into a cryogenically cooled 3D Paul trap operated at 4.6 K by a series of radio-frequency ion guides. After being accumulated for about 0.1 s and thermally cooled via collisions with a mixed background gas of He/H_2 (4/1 in volume),[4] the anions were unloaded from the trap at a 10 Hz repetition rate and focused into the extraction zone of a modified Wiley-McLaren time-of-flight mass spectrometer. The *p*-EP$^-$ anions were selected by a mass gate and focused into the interaction zone of a multilens high-resolution VMI system,[51] where the anions were intercepted by the detachment laser beam, from either a tunable dye laser or a Nd:YAG laser. Photoelectrons were extracted and accelerated from the interaction zone and projected onto a pair of 75 mm diameter microchannel plates coupled to a phosphor screen and captured by a charge-coupled device camera. Photoelectron images were inverse-Abel transformed and reconstructed using the pBasex and BASEX programs.[55,56] The photoelectron images were calibrated using Au$^-$ at different photon energies. The kinetic energy (KE) resolution was 3.8 cm^{-1} for electrons with 55 cm^{-1} KE and about 1.5% (ΔKE/KE) for KE above 1 eV in the current experiment. The resolution of the photoelectron images depends on the extraction voltage on the imaging lens. Lower extraction voltages give better resolution, but higher extraction voltages are needed for the detection of fast electrons. In the current experiment, the extraction voltage used was 300 V for all of the experiment, except for the R2PD experiment, where a higher voltage (1000 V) was used to detect fast electrons.

Geometry optimization, electronic structure calculations, and the calculation of the dipole moment of *p*-EP were performed using density functional theory (DFT) at the B3LYP/aug-cc-pVTZ level. The electronic structure calculations were followed by vibrational analyses. All calculations were done using the Gaussian 09 package.[57]

3. RESULTS

3.1. Nonresonant Photoelectron Imaging and Spectroscopy

Figure 1 shows six nonresonant photoelectron images and spectra of *p*-EP$^-$ with increasing photon energies. Thirteen peaks, labeled as $0_0{}^0$ and A−L, are resolved, corresponding to the vibrational levels of the *p*-EP neutral in its ground electronic state. The lowest binding energy peak ($0_0{}^0$) defines the detachment threshold of the *p*-EP$^-$ anion or EA of the *p*-EP radical. The near-threshold spectrum at 2.1615 eV (Figure 1a) yields the most accurate EA as 2.1604 ± 0.0004 eV (17425 ± 3 cm^{-1}). The positions of peaks $0_0{}^0$ and A−L are summarized in Table 1. Figure 1 demonstrates vividly the tremendous advantage of cryogenic ion cooling in obtaining high-resolution photoelectron spectra of complex anions, in comparison to the previous PES study of the same anion, where no vibrational structures were resolved and the EA of *p*-EP was not reported.[54] The rotational temperature of anions in our ion trap was estimated to be ~30 K previously.[28,58,59] Assuming a similar vibrational temperature, there should be non-negligible population of the lowest-frequency mode of *p*-EP$^-$ (ν_{48} at 43 cm^{-1}, Table S2). Indeed, a very weak tail can be seen on the lower binding energy side of the $0_0{}^0$ transition in Figure 1a−c, which should be due to the hot band transition of the ν_{48} mode. However, this very weak hot band is so weak that it does not cause any spectral congestion.

Table 1. Binding Energies (BEs) of the Observed Vibrational Peaks in the Photoelectron Spectra of *p*-EP$^-$, Their Shifts from the 0−0 Transition, and Assignments[a]

peak	BE (eV)[b]	BE (cm^{-1})[b]	shift (cm^{-1})	assignment	calculation (cm^{-1})[c]
$0_0{}^0$	2.1604 (4)	17425 (3)	0		
A	2.1714(6)	17514(5)	89	27^1	89
B	2.1847(4)	17621(3)	196	26^1	200
C	2.1957(4)	17710(3)	285	$27^1 26^1$	289
D	2.2037(4)	17774 (3)	349	25^1	348
E	2.2172(4)	17883(3)	458	24^1	456
F	2.2274(5)	17965(4)	540	$23^1/26^1 25^1$	537/548
G	2.2415(6)	18079(5)	654	$26^1 24^1$	656
H	2.2490(6)	18140(5)	715	22^1	710
I	2.2521(7)	18165(6)	740	$21^1/26^1 23^1$	745/737
J	2.2605(6)	18232(5)	807	$25^1 24^1$	804
K	2.2740(5)	18341(4)	916	24^2	912
L	2.2838(8)	18420(6)	995	$24^1 23^1/$ $26^1 25^1 24^1$	993/1004
a	2.1646(8)	17459(6)	34	48^1	36
b	2.1690(8)	17494(6)	69	48^2	72
c	2.1825(8)	17603(6)	178	27^2	178
d	2.1889(10)	17655(8)	230	$48^1 26^1$	236
e	2.2059(9)	17792(7)	367	$48^1 46^1$	362
f	2.2090(9)	17817(7)	392	26^2	400
g	2.2147(9)	17863(7)	438	$27^1 25^1$	437
h	2.2354(7)	18030(6)	605	43^1	608
i	2.2380(15)	18051(12)	626	$27^1 23^1$	626
j	2.2469(12)	18123(10)	698	25^2	696
k	2.2580(9)	18212(7)	787	$27^1 25^2$	785
l	2.2655(8)	18273(6)	848	19^1	849
m	2.2782(9)	18375(8)	950	18^1	937

[a]The theoretical frequencies (Table S1) of the relevant vibrational modes of *p*-EP are given for comparison. [b]Numbers in parentheses indicate the experimental uncertainties in the last digit. [c]Calculated frequencies are scaled by a factor of 0.975.

3.2. Photodetachment Spectroscopy

The dipole moment of *p*-EP is calculated in the present study to be 4.85 D at the B3LYP/aug-cc-pVTZ level of theory. A slightly larger value was reported previously using a smaller basis set (B3LYP/aug-cc-pVDZ).[54] These values were larger

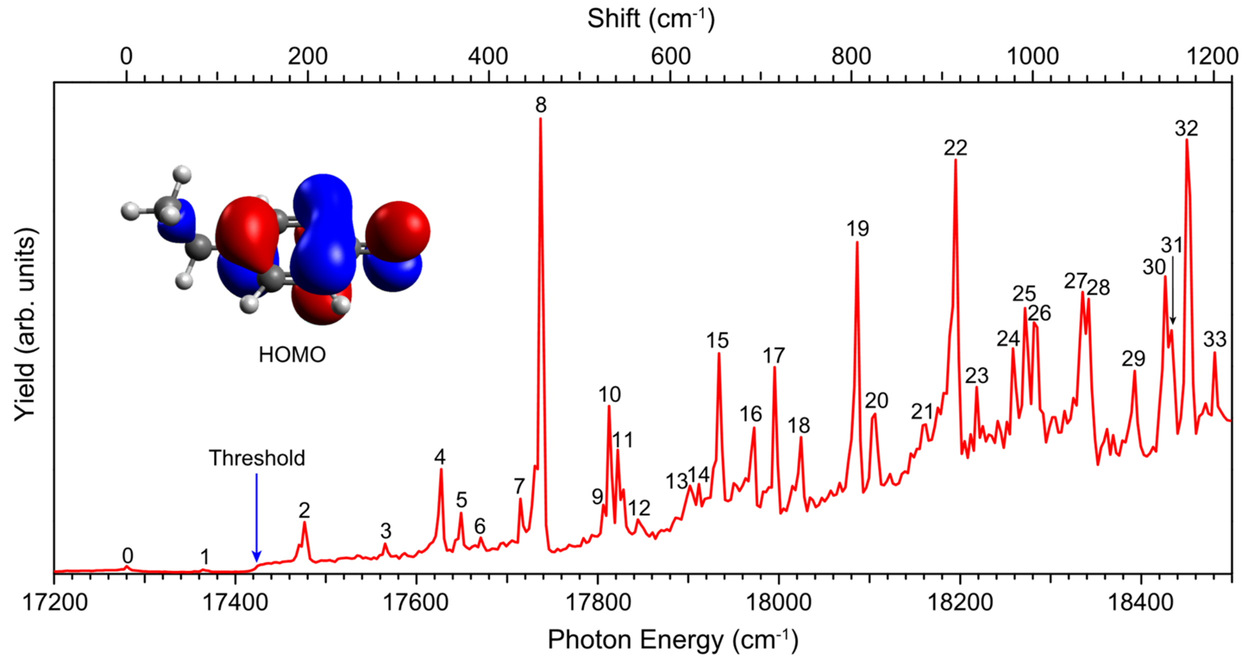

Figure 2. Photodetachment spectrum of *p*-EP$^-$. The inset shows the HOMO of *p*-EP$^-$.

than the empirical critical value of 2.5 D for the existence of a DBS as an excited electronic state for a valence-bound anion.[24] An excited DBS was indeed observed for *p*-EP$^-$ in the previous low-resolution photodetachment study at room temperature, though the binding energy of the DBS was not obtained.[54] Our high-resolution photodetachment spectrum of cold *p*-EP$^-$ using cryogenic cooling is presented in Figure 2 in the photon energy range between 17200 and 18500 cm^{-1} (2.1325−2.2937 eV). A clear step is observed at the detachment threshold of 17425 cm^{-1} (2.1604 eV) (marked by an arrow), consistent with the s-partial wave character of photoelectrons detached from the π-type HOMO (inset of Figure 2) of *p*-EP$^-$ following the Wigner threshold law.[60] The observed peaks (0−33) are all due to transitions to the vibrational levels of the DBS. The two below-threshold peaks (0 and 1) are due to R2PD processes, whereas peaks 2−33 are vibrational Feshbach resonances. Peak 0 at 17280 cm^{-1} (2.1424 eV) should correspond to the zero-point level of the DBS because there is no more transition at lower photon energies. The binding energy of the DBS is measured to be 145 cm^{-1} (0.0180 eV) defined by the energy separation between peak 0 and the detachment threshold. The Feshbach resonances (peaks 2−33) correspond to single-photon transitions to vibrational levels of the DBS followed by vibrational autodetachment. The laser wavelengths, photon energies of peaks 0−33, and the shifts relative to peak 0 are given in Table 2.

3.3. R2PD Photoelectron Imaging

By setting the detachment laser wavelength at the positions of the bound levels (0 and 1 in Figure 2) of the DBS, the R2PD images and spectra are obtained, as presented in Figure 3. The low binding energy feature (labeled "DBS") is due to the direct detachment of the dipole-bound electron by a second photon within the same laser pulse (~5 ns), i.e., a single-color R2PD process, which probes the nature of the DBS. The *p*-wave character of the "DBS" peak (the outmost ring) with an anisotropy parameter (β) of 1.1 ± 0.1 confirms the σ-type orbital of the DBS. Since the "DBS" feature at peak 1 is too weak relative to feature "S_0" (Figure 3a), the outer ring is not visible with the current contrast in the image of Figure 3a. The sharp intense feature "S_0" at the high binding energy side should be due to detachment from rovibrationally excited states of the *p*-EP$^-$ anion in its ground electronic state, populated by relaxation from the DBS after absorbing the first photon.[38,44]

3.4. Resonant PES of *p*-EP$^-$ via the Vibrational Feshbach Resonances

By setting the wavelengths of the detachment laser to the positions of the Feshbach resonances (peaks 2−33) in Figure 2, 32 resonant photoelectron images and spectra are obtained. These data are classified into four categories based on the types of vibrational excitations, as shown in Figures 4−7. Since first realized for the phenoxide anion in 2013,[27] rPES via DBS of cryogenically cooled anions has proven to be extremely powerful for obtaining spectroscopic information on neutral radical species.[6,28−49] Compared to the nonresonant photoelectron spectra in Figure 1, one or more transitions are enhanced in the resonant spectra (labeled in bold face in Figures 4−7) and in some resonant spectra new peaks appear (labeled as lowercase letters). The binding energies of the new peaks observed in the resonant photoelectron spectra, their shifts to the detachment threshold, and assignments are also given in Table 1. The binding energies in Table 1 for the FC-active vibrational peaks observed in Figure 1 are all from the rPES data, where they are measured more accurately.

4. DISCUSSION

4.1. Nonresonant Photoelectron Spectra of *p*-EP$^-$

The photoelectron spectra of *p*-EP$^-$ (Figure 1) are considerably more complicated in comparison with that of the parent phenoxide,[27,36,61,62] due to the reduced symmetry (C_s) and the additional vibrational modes, in particular, low-frequency modes related to the ethyl group. The computed FC factors for the detachment transition from the anion ground state to that of the neutral *p*-EP radical are compared with the

Table 2. Observed DBS Vibrational Peaks in the Photodetachment Spectrum of p-EP$^-$, with Their Wavelengths, Photon Energies, Shifts Relative to the Ground Vibrational Level, and Assignments

peak	wavelength (nm)	photon energy (eV)	photon energy (cm^{-1})	shift (cm^{-1})	assignment
0	578.72	2.1424	17280	0	ground state of DBS
1	575.90	2.1529	17364	84	$27'^{1}$
2	572.23	2.1667	17475	195	$26'^{1}$
3	569.32	2.1778	17565	285	$27'^{1}26'^{1}$
4	567.38	2.1852	17625	345	$25'^{1}$
5	566.66	2.1880	17647	367	$48'^{1}46'^{1}/27'^{2}26'^{1}$
6	565.88	2.1910	17672	392	$26'^{2}$
7	564.50	2.1964	17715	435	$27'^{1}25'^{1}$
8	563.80	2.1991	17737	457	$24'^{1}$
9	561.55	2.2079	17808	528	$48'^{2}24'^{1}$
10	561.32	2.2088	17815	535	$23'^{1}$
11	561.10	2.2097	17822	542	$26'^{1}25'^{1}$
12	560.38	2.2125	17845	565	$48'^{1}26'^{1}46'^{1}$
13	558.56	2.2197	17903	623	$27'^{1}23'^{1}$
14	558.30	2.2207	17912	632	$27'^{1}26'^{1}25'^{1}$
15	557.62	2.2235	17933	653	$26'^{1}24'^{1}$
16	556.46	2.2281	17971	691	$25'^{2}$
17	555.71	2.2311	17995	715	$22'^{1}/27'^{2}26'^{1}25'^{1}$
18	554.85	2.2346	18023	743	$27'^{1}26'^{1}24'^{1}/$ $21'^{1}/26'^{2}25'^{1}$
19	552.94	2.2423	18085	805	$25'^{1}24'^{1}/43'^{1}26'^{1}$
20	552.28	2.2450	18107	827	$48'^{1}46'^{1}24'^{1}$
21	550.66	2.2516	18160	880	$25'^{1}23'^{1}$
22	549.64	2.2557	18194	914	$24'^{2}$
23	548.89	2.2588	18219	939	$26'^{1}21'^{1}$
24	547.71	2.2637	18258	978	$27'^{1}26'^{1}25'^{2}/$ $27'^{1}25'^{1}23'^{1}$
25	547.32	2.2653	18271	991	$24'^{1}23'^{1}$
26	547.01	2.2666	18281	1001	$26'^{1}25'^{1}24'^{1}$
27	545.47	2.2730	18333	1053	$15'^{1}$
28	545.26	2.2739	18340	1060	$25'^{1}22'^{1}/43'^{1}24'^{1}/$ $47'^{1}19'^{1}/$ $48'^{2}24'^{1}23'^{1}$
29	543.74	2.2802	18391	1111	$26'^{1}24'^{2}$
30	542.70	2.2846	18426	1146	$14'^{1}$
31	542.55	2.2852	18431	1151	$25'^{2}24'^{1}$
32	541.95	2.2877	18452	1172	$24'^{1}22'^{1}/$ $48'^{2}26'^{1}24'^{2}/$ $45'^{1}25'^{1}24'^{1}$
33	541.13	2.2912	18480	1200	$24'^{1}21'^{1}$

spectrum at 2.2892 eV in Figure 8. The theoretical frequencies used in the FC calculations (Figure S1 and Table S1) are scaled by a factor of 0.975. The good agreement between the computed FC factors and the experimental data allows all the observed vibrational peaks to be readily assigned, as summarized in Table 1. The ν_{24} mode (Figure S1) is the most FC-active mode, consisting of E (24^1) and K (24^2), reminiscent of the ν_{11} mode in the photoelectron spectra of the parent phenoxide.[27,36,61,62] Additionally, peaks A (27^1), B (26^1), D (25^1), and H (22^1) come from fundamental excitations of p-EP, whereas peaks C ($27^1 26^1$), G ($26^1 24^1$), and J ($25^1 24^1$) are due to combinational modes of p-EP. Several peaks are assigned to multiple transitions, F ($23^1/26^1 25^1$), I ($21^1/26^1 23^1$), and L ($24^1 23^1/26^1 25^1 24^1$), on the basis of the FC simulation. All the observed vibrational modes are allowed under C_s symmetry (A′) (Figure S1 and Table S1).

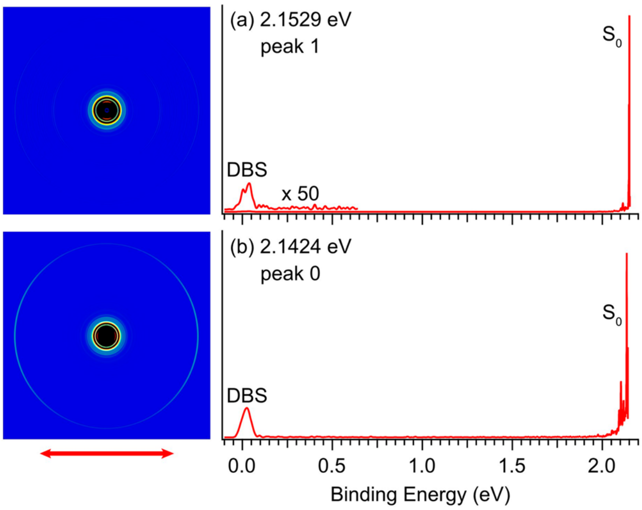

Figure 3. R2PD images and spectra of p-EP$^-$ at (a) 2.1529 eV (17364 cm^{-1}, peak 1 in Figure 2) and (b) 2.1424 eV (17280 cm^{-1}, peak 0 in Figure 2). The double arrow below the images indicates the direction of the laser polarization.

4.2. Binding Energy of the DBS in p-EP$^-$

The binding energies of DBS as a function of dipole moments were systematically investigated for a series of *para*-halogen-substituted phenoxide anions (p-$XC_6H_4O^-$, X = F, Cl, Br, and I).[24] The dipole moments of the corresponding neutral radicals range from 2.56 to 4.06 D. Because of the similarity in molecular structures and size, these anions provided ideal systems to evaluate the charge-dipole interactions on the electron binding energies in their DBSs, while minimizing molecule-dependent effects. The binding energies (BE) in cm^{-1} were found to be linearly dependent on the dipole moment for this set of molecules with a fitted function of BE = $63.4\mu - 159.0$, which gives a $\mu_{\text{critical}} = 2.5$ D for BE = 0.[24] The p-EP radical is similar to the halogen substituted phenoxy radicals and should follow this equation. Indeed, this equation predicts a BE of 148 cm^{-1} for the DBS of p-EP, in excellent agreement with the measured BE of 145 ± 3 cm^{-1}. This result confirms again the validity of the empirical critical dipole moment of 2.5 D for the existence of a DBS. The critical dipole moment can be further tested using different isomers of substituted phenoxides.

4.3. Comparison between the Photodetachment and Photoelectron Spectra of p-EP$^-$

Since the diffuse dipole-bound electron has little influence on the geometry of the neutral core, photodetachment spectra of DBSs have been found to resemble photoelectron spectra,[6] which are governed by the Franck-Condon principle. The photoelectron spectrum of p-EP$^-$ at 2.2892 eV (Figure 1f) is overlaid on the photodetachment spectrum in Figure 9 by aligning peak 0_0^0 with peak 0. It can be readily seen that major peaks of the photodetachment spectrum agree well with the vibrational peaks in the photoelectron spectrum, except that the resolution of the photodetachment spectrum is much higher. The one-to-one correspondence between the two types of spectra is labeled in Figure 9. The similarity between the two types of spectroscopy is a direct confirmation that the neutral structure of p-PE is similar to that of p-EP$^-$ in the DBS, and that they have parallel potential energy surfaces and similar vibrational frequencies. Thus, the DBS vibrational levels can be

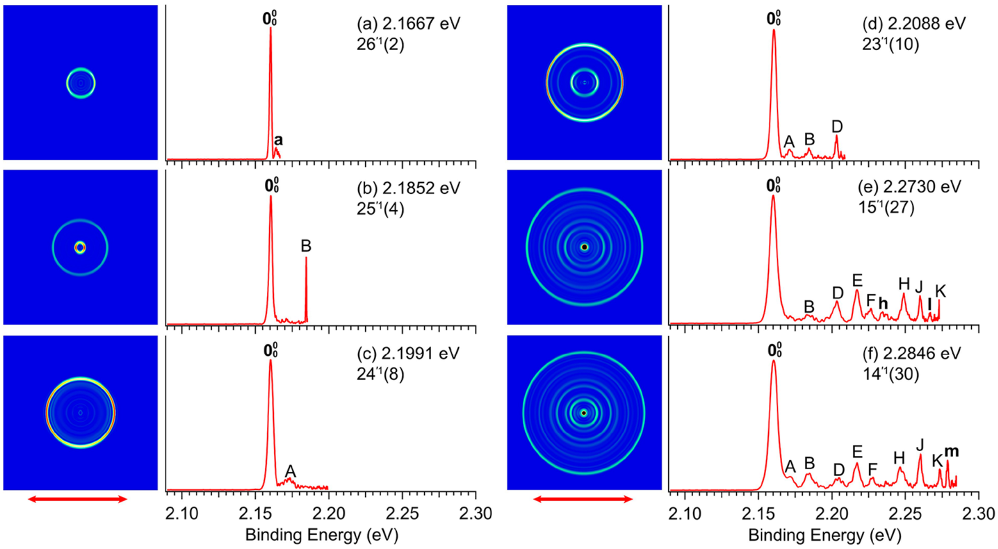

Figure 4. Resonant photoelectron images and spectra of *p*-EP$^-$ at (a) 2.1667 eV (17475 cm^{-1}), (b) 2.1852 eV (17625 cm^{-1}), (c) 2.1991 eV (17737 cm^{-1}), (d) 2.2088 eV (17815 cm^{-1}), (e) 2.2730 eV (18333 cm^{-1}), and (f) 2.2846 eV (18426 cm^{-1}). The assignment of the excited DBS level is given and the number in the parentheses after the assignment is the resonant peak number in Figure 2. The double arrows below the images indicate the direction of laser polarization.

assigned using the assignments of the PES features. For example, peak 2 is assigned to $26'^1$ of the DBS (the prime $'$ is used to denote vibrational modes of the DBS) because peak B in the photoelectron spectrum is due to 26^1 (Table 1). Additional weak peaks are observed in the photodetachment spectrum that do not have corresponding transitions in the photoelectron spectrum because of the high sensitivity of the resonant optical excitation to the DBS in PDS. The additional transitions in the photodetachment spectrum contain new vibrational information about the neutral final state. Furthermore, the Feshbach resonances can be assigned from the resonant photoelectron spectra according to the $\Delta v = -1$ autodetachment propensity rule, as will be discussed below.

4.4. R2PD via the Bound Vibrational Levels of the DBS

In 2013, we carried out the first R2PD photoelectron imaging study on the DBS of the cryogenically cooled phenoxide anion.[27] The sequential R2PD photoelectrons present distinct *p*-wave angular distribution, consistent with the σ-type dipole-bound orbital of the phenoxide anion. The first π-type DBS was observed in the 9-anthrolate anion based on a distinct (s+d)-wave character of the sequential R2PD signals.[40] With the help of the accurately measured energetic information, pump-probe studies have been successfully conducted to probe the lifetime and dynamics of Feshbach resonances in the DBS of phenoxide.[63] The "DBS" feature in Figure 3b exhibits a beautiful p-wave angular distribution, consistent with the expected σ-type DBS for *p*-EP$^-$. Since the dipole-bound electron has little effect to the geometry of the neutral core, photodetachment from the DBS to the neutral is strictly adiabatic, i.e., there is no vibrational energy change between the initial and final state during the detachment process. Therefore, a single-peak "DBS" feature is observed in the R2PD spectra without any vibrational progression (Figure 3), again confirming the structure of the DBS is the same as the neutral final state. The adiabatic detachment behavior from DBS to neutral has been systematically investigated previously using R2PD.[38,45] PES of ground state DBSs has also shown similar adiabatic behaviors.[64]

The high binding energy feature labeled "S$_0$" in Figure 3 come from photodetachment of rovibrational states of the ground state (S$_0$) of the *p*-EP$^-$ anion. Since the anions are cooled in the cryogenic ion trap, the rovibrationally excited states of *p*-EP$^-$ must come from relaxation processes upon the absorption of the first photon. The relaxation should happen within the 5 ns laser pulse, so that the nascent excited anions can be detached by the second photon of the same laser pulse. The zero-point level or the bound vibrational excited state of the DBS should be long-lived. However, relaxation on the nanosecond time scale from DBSs to valence-bound states has been observed quite often in R2PD photoelectron imaging.[38,45] In contrast, the Feshbach resonances have lifetimes on the order of picoseconds due to autodetachment via vibronic coupling. The autodetachment dynamics of Feshbach resonances in DBS have been probed recently using picosecond pump-probe experiments.[63,65]

4.5. Resonant Photoelectron Images and Spectra via the Vibrational Feshbach Resonances

Two processes contribute to the rPES at the Feshbach resonances of the DBS: the nonresonant direct detachment process and the resonantly enhanced vibrational autodetachment. The $\Delta v = -1$ propensity rule suggests that only one vibrational quantum can be coupled to the dipole-bound electron during autodetachment under the harmonic oscillator approximation.[25,26] For example, if a resonant excitation occurs to the DBS vibrational level $\nu_x'^n$ (the nth quantum of the ν_x' mode), autodetachment will lead to the enhancement of the (n−1)th level of the same vibrational mode in the neutral (ν_x^{n-1}). For autodetachment from a combinational level ($\nu_x'^n\nu_y'^m$...) of the DBS, the final neutral state can be either $\nu_x'^{n-1}\nu_y'^m$... or $\nu_x'^n\nu_y'^{m-1}$..., producing multiple enhanced vibrational peaks in rPES. Thus, one or more vibrational final states are enhanced in the resonant photoelectron spectra, which are highly non-Franck-Condon in comparison with the nonresonant photoelectron spectra in Figure 1. The autodetachment propensity rule can provide a valuable guide for spectral assignment, although violation of the $\Delta v = -1$

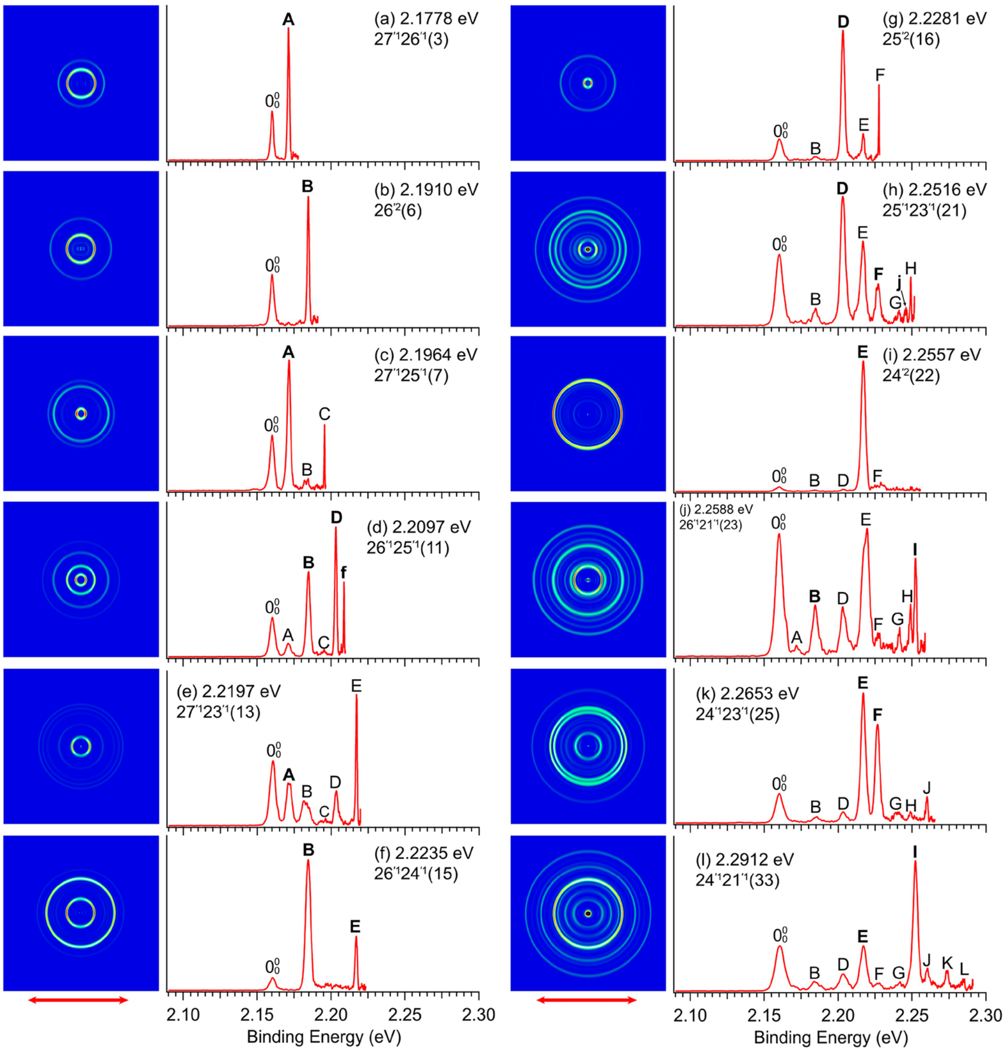

Figure 5. Resonant images and spectra of *p*-EP⁻ at (a) 2.1778 eV (17565 cm^{-1}), (b) 2.1910 eV (17672 cm^{-1}), (c) 2.1964 eV (17715 cm^{-1}), (d) 2.2097 eV (17822 cm^{-1}), (e) 2.2197 eV (17903 cm^{-1}), (f) 2.2235 eV (17933 cm^{-1}), (g) 2.2281 eV (17971 cm^{-1}), (h) 2.2516 eV (18160 cm^{-1}), (i) 2.2557 eV (18194 cm^{-1}), (j) 2.2588 eV (18219 cm^{-1}), (k) 2.2653 eV (18271 cm^{-1}), and (l) 2.2912 eV (18480 cm^{-1}). The assignment of the excited DBS level is given and the number in the parentheses after the assignment is the resonant peak number in Figure 2. The double arrows below the images indicate the direction of laser polarization.

propensity rule can occur as a result of anharmonicity[25] and has been observed often for low-frequency bending modes.[35] For excitations to combinational or overlapping vibrational levels of the DBS, the resulting resonant photoelectron spectra can be quite complicated, containing rich vibrational information that would not be assessible in nonresonant PES. Using the autodetachment propensity rule, comparison between the photodetachment and photoelectron spectra (Figure 9), and the calculated vibrational frequencies of *p*-EP (Table 1), we are able to assign all the vibrational levels of the DBS observed the photodetachment spectrum (Figure 2).

4.5.1. Excitation to Fundamental Vibrational Levels of the DBS and the Observation of Intramolecular Rescattering Effects. According to the $\Delta v = -1$ propensity rule, excitation to fundamental vibrational levels of the DBS ($\nu_x{'}^1$) leads to the enhancement of the 0_0^0 transition, as shown in Figure 4 for the spectra taken at Feshbach resonances 2, 4, 8, 10, 27, and 30. By comparing the excitation energies of the Feshbach resonances (Table 2) with the theoretical frequencies (Table S1), we can readily assign them to fundamental vibrational modes of the DBS. The excitation energies of peaks 2, 4, 8, 10, 27, and 30 are 195, 345, 457, 535, 1053, and 1146 cm^{-1}, respectively (Table 2), in good agreement with the calculated frequencies of the neutral vibrational modes 26^1 (200 cm^{-1}), 25^1(348 cm^{-1}), 24^1(456 cm^{-1}), 23^1(537 cm^{-1}), 15^1(1040 cm^{-1}), and 14^1(1141 cm^{-1}). All these modes are of A′ symmetry (Figure S1), which are FC-allowed for *p*-EP with C_s geometry. The assignments of peaks 2, 4, 8, and 10 are further confirmed by the comparison between the photodetachment and the nonresonant photoelectron spectrum (Figure 9), where peaks 2, 4, 8, and 10 in the photodetachment spectrum are aligned with peaks B (26^1), D (25^1), E (24^1), and F ($23^1/26^1 25^1$), respectively, in the nonresonant photoelectron spectra.

Besides the expected enhancement of the 0_0^0 transition, some new peaks are also observed, e.g., the weak peak **a** in Figure 4a, peaks **h** and **l** in Figure 4e, and peak **m** in Figure 4f, which are absent in the nonresonant spectra (Figure 1). The new peaks **h**/**l** and **m** should be contributed by the nearby Feshbach resonances 28 and 31 (Figure 2), which are partially overlapped with Feshbach resonances 27 and 30, respectively. Hence, the assignments of peaks **h** (43^1), **l** (19^1), and **m** (18^1)

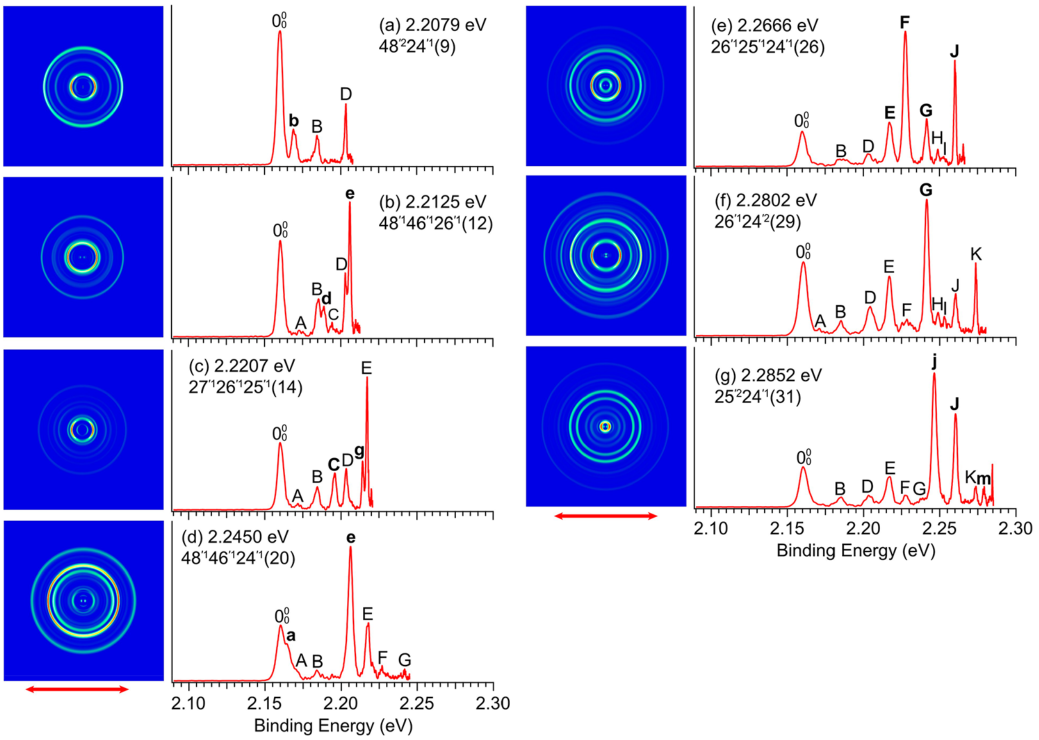

Figure 6. Resonant photoelectron images and spectra of *p*-EP⁻ at (a) 2.2079 eV (17808 cm^{-1}), (b) 2.2125 eV (17845 cm^{-1}), (c) 2.2207 eV (17912 cm^{-1}), (d) 2.2450 eV (18107 cm^{-1}), (e) 2.2666 eV (18281 cm^{-1}), (f) 2.2802 eV (18391 cm^{-1}), and (g) 2.2852 eV (18431 cm^{-1}). The assignment of the excited DBS level is given and the number in the parentheses after the assignment is the resonant peak number in Figure 2. The double arrows below the images indicate the direction of laser polarization.

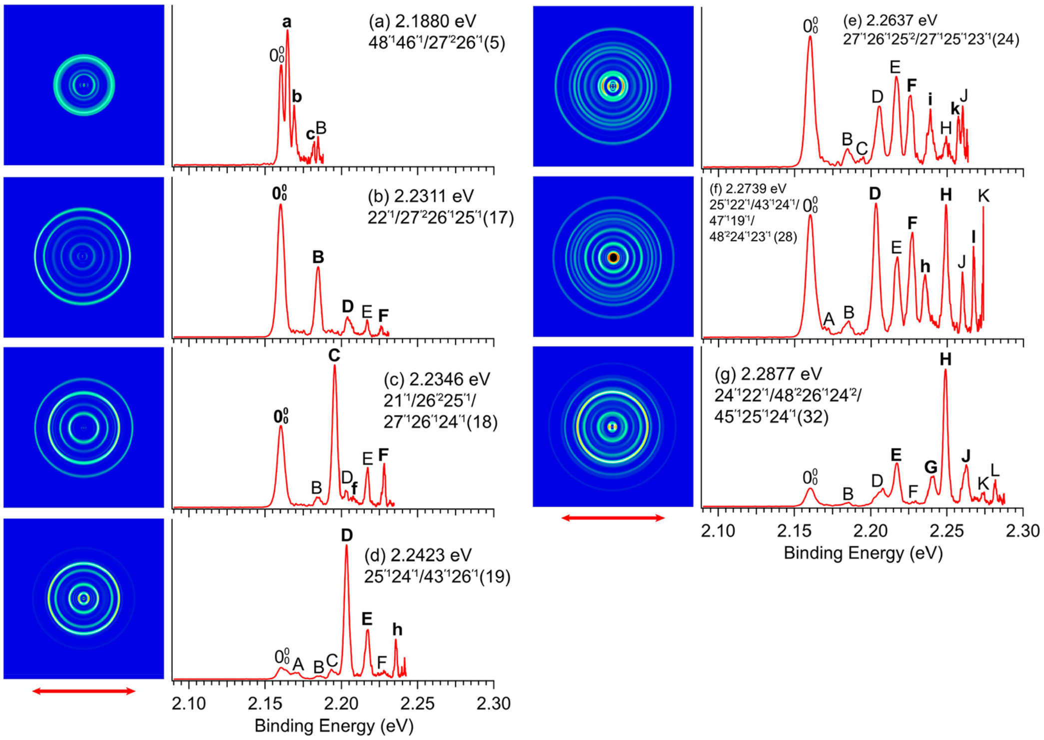

Figure 7. Resonant photoelectron images and spectra of *p*-EP⁻ at (a) 2.1880 eV (17647 cm^{-1}), (b) 2.2311 eV (17995 cm^{-1}), (c) 2.2346 eV (18023 cm^{-1}), (d) 2.2423 eV (18085 cm^{-1}), (e) 2.2637 eV (18258 cm^{-1}), (f) 2.2739 eV (18340 cm^{-1}), and (g) 2.2877 eV (18452 cm^{-1}). The assignment of the excited DBS level is given and the number in the parentheses after the assignment is the resonant peak number in Figure 2. The double arrows below the images indicate the direction of laser polarization.

will be discussed in the following when the rPES related to Feshbach resonances 28 and 31 is presented. The weak peak **a** in the spectrum of Figure 4a has a binding energy of 2.1646 eV (17459 cm^{-1}), with an energy shift of 34 cm^{-1} to the 0_0^0

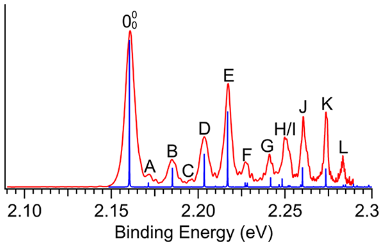

Figure 8. Comparison of the calculated FC factors with the photoelectron spectrum of *p*-EP$^-$ at 2.2892 eV.

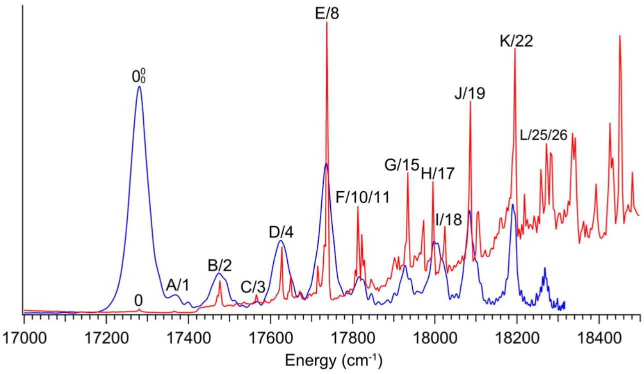

Figure 9. Comparison of the nonresonant PE spectrum at 2.2892 eV (blue) with the photodetachment spectrum (red). The PE spectrum is red-shifted by 145 cm^{-1} to align peak 0_0^0 with peak 0 of the photodetachment spectrum.

transition. According to the calculated frequency shown in Table S1, peak **a** could only be assigned to the lowest-frequency mode 48^1 (A″), involving the ethyl group (Figure S1). This weak vibrational feature could not come from autodetachment of the $26'^1$ DBS vibrational level. The appearance of peak **a** (48^1) is most likely caused by the intramolecular inelastic rescattering effect, i.e., the autodetached electron with a kinetic energy of 50 cm^{-1} (195−145 cm^{-1}) is inelastically scattered off the neutral core by exciting the ν_{48} mode. The intramolecular inelastic rescattering effect of an autodetached dipole-bound electron has been invoked previously to explain unexpected excitations of low-frequency vibrational modes in rPES.[35] Low-frequency modes are expected to exhibit stronger inelastic scattering effects because of their large amplitude motions. Peak **a** may also exist in other resonant photoelectron spectra at higher photon energies, but it can only be resolved near threshold in the resonant spectrum taken at Feshbach resonance $26'^1$.

4.5.2. Excitation to Combinational or Overtone Levels of the DBS. The majority of the Feshbach resonances observed in Figure 2 involve combinational or overtone vibrational levels of the DBS (Table 2). Figure 5 displays the resonant photoelectron spectra for DBS levels of two vibrational quanta, either a combinational level ($\nu_x'^1\nu_y'^1$) or an overtone ($\nu_x'^2$). Both the vibrational final states, ν_x^1 or ν_y^1, may be enhanced for the former, whereas the ν_x^1 final state will be enhanced for the latter, according to the $\Delta\nu = -1$ propensity rule. For example, Feshbach resonance 3 in the photodetachment spectrum is due to the $27'^126'^1$ DBS level on the basis of its alignment with peak C (27^126^1) in the photoelectron spectrum (Figure 9). Thus, the final state peak A (27^1) is highly enhanced via the coupling of the vibrational quantum of the ν_{26}' mode ($26'^1$) (Figure 5a). On the other hand, the $27'^1$ quantum (84 cm^{-1}, Table 2) is too small to induce autodetachment relative to the DBS binding energy (145 cm^{-1}). The same situation happens in Figure 5c,e, where the strong enhancement of peak A (27^1) is due to excitation of the combinational DBS levels of $27'^125'^1$ and $27'^123'^1$, respectively. The enhancement of the final state B (26^1) in Figure 5b is due to the excitation of the $26'^2$ overtone DBS level. Similarly, the strong enhancement of the final states D (25^1) in Figure 5g and E (24^1) in Figure 5i are also due to excitations to overtone DBS levels.

In Figure 5d, both final states B (26^1) and D (25^1) are enhanced as a result of excitation to the $26'^125'^1$ DBS level. The coupling of the $25'^1$ quantum to the dipole-bound electron leads to the enhancement of the B final state, whereas the coupling of the $26'^1$ quantum results in the enhancement of the D final state. Similarly, the enhancement of two vibrational final states in Figure 5f (B and E), 5h (D and F), 5j (B and I), 5k (E and F), and 5l (E and I) are all due to excitation to combinational levels of the DBS with two vibrational quanta ($\nu_x'^1\nu_y'^1$). It is interesting to note that there is no strong mode selectivity in the autodetachment process in these cases, unlike in the parent phenoxide, where strong mode selectivity was first observed.[27] Additionally, new features are observed in several resonant photoelectron spectra, relative to the nonresonant spectra in Figure 1. Peak **f** observed in Figure 5d near threshold is due to 26^2, which is not resolved in Figure 1 because of its small FC factor (Figure 8) and the limited spectral resolution. The weak peak **j** in Figure 5h is due to 25^2, suggesting that a weak unresolved DBS level $26'^125'^2$ may contribute to the Feshback resonance 21 ($25'^123'^1$), which is separated by only 5 cm^{-1}. Resonant spectra involving more prominent overlapping DBS levels are gathered in Figure 7 (vide infra).

4.5.3. Excitation to Combinational Levels of the DBS with Three Vibrational Quanta. Figure 6 displays resonant photoelectron spectra involving transitions to combinational DBS levels of three vibrational quanta with three ($\nu_x'^1\nu_y'^1\nu_z'^1$) or two ($\nu_x'^2\nu_y'^1$) different modes. For example, Figure 6a is assigned to excitation to the DBS level $48'^224'^1$, resulting in the appearance of the new peak **b** (48^2) at 2.1690 eV (17494 cm^{-1}) due to the coupling of the $24'^1$ vibrational quantum to the dipole-bound electron. The $48'^1$ quantum (34 cm^{-1}) is too small to induce autodetachment. In Figure 6b, two new peaks **d** (48^126^1) and **e** (48^146^1) appear as a result of excitation to the $48'^146'^126'^1$ DBS level and autodetachment via the coupling of the $46'^1$ or $26'^1$ quantum to the dipole-bound electron, respectively. The situation in Figure 6c is similar, due to excitation of the $27'^126'^125'^1$ DBS level. Because the $27'^1$ quantum (84 cm^{-1}) is too small to induce autodetachment, only two enhanced peaks are observed: C (27^126^1) and a new peak **g** (27^125^1) (Table 1). In Figure 6d, the strong enhancement of the final state **e** (48^146^1) suggests excitation to the $48'^146'^124'^1$ DBS level via coupling of the $24'^1$ quantum to the dipole-bound electron. Interestingly, there is a mode selectivity in the autodetachment from this DBS level because the expected 48^124^1 final state via the coupling of the $46'^1$ quantum is not observed. Furthermore, the observation of the final state **a** (48^1) indicates a violation of the $\Delta\nu = -1$ propensity rule because two vibrational quanta ($46'^124'^1$) are coupled to the dipole-bound electron to produce this final state. The enhancement of the final states F (26^125^1), G (26^124^1), and J (25^124^1) in Figure 6e are all expected from the excitation of the $26'^125'^124'^1$ DBS level according to the

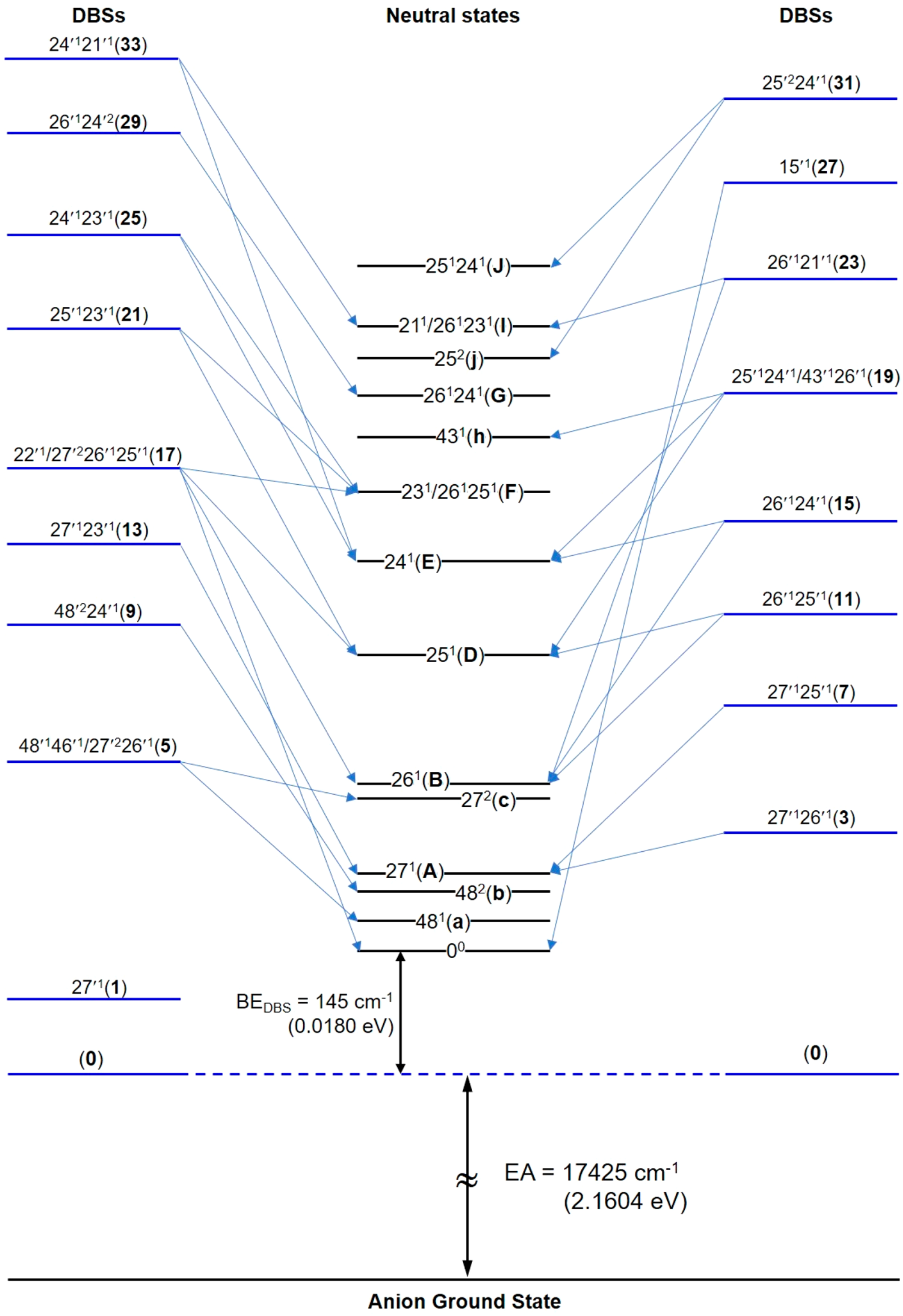

Figure 10. Schematic energy level diagram for autodetachment from the DBS vibrational levels (odd peak number in the photodetachment spectrum in Figure 2) of *p*-EP$^-$ to the neutral final states.

propensity rule. The slight enhancement of the final state E (24^1) could be due to the violation of the propensity rule, similar to the enhancement of peak **a** in Figure 6d. The spectrum in Figure 6f is due to excitation to the $26'^1 24'^2$ DBS level, and it also displays a strong mode dependence. The prominently enhanced final state G ($26^1 24^1$) indicates a strong coupling of the ν_{24}' mode with the dipole-bound electron, whereas the final state K (24^2) is not significantly enhanced, suggesting that the ν_{26}' mode is not strongly coupled. The appearance of the new peak **j** (25^2) and the strongly enhanced final state J ($25^1 24^1$) in Figure 6g both follow the propensity rule as a result of the excitation to the $25'^2 24'^1$ DBS level. The appearance of the peak **m** (18^1) in both Figure 4f and Figure 6g is likely due to a weak unresolved DBS level $26'^2 18'^1$, which would overlap with both peaks 30 and 31 in the photodetachment spectrum. With such a complicated molecular system, the vibrational density of states is expected to increase rapidly with excitation energies, as revealed in the resonant photoelectron spectra in Figure 7.

4.5.4. Excitation to Overlapping Levels of the DBS.

Figure 7 presents more complicated resonant photoelectron spectra due to overlapping DBS levels. These data illustrate the power of high-resolution rPES for providing rich vibrational information for the neutral final states that is not accessible in conventional PES. Surprisingly, the spectrum taken at Feshbach resonance 5 (Figure 7a) exhibits complicated and unexpected features, even though the excitation energy is only 367 cm^{-1} above the zero-point level of the DBS. Specifically,

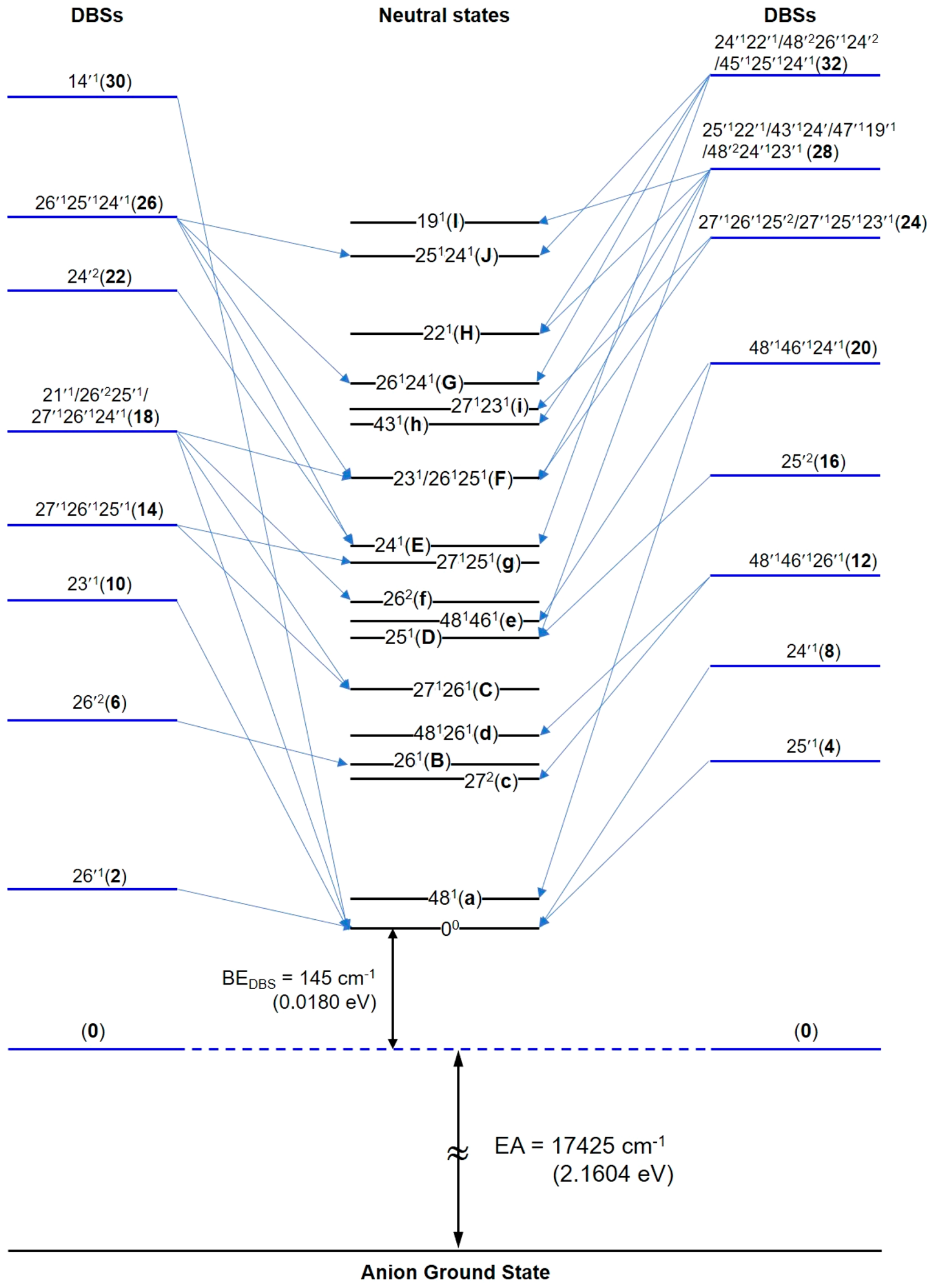

Figure 11. Schematic energy level diagram for autodetachment from the DBS vibrational levels (even peak number in the photodetachment spectrum in Figure 2) of *p*-EP$^-$ to the neutral final states.

the final states **a** (48^1) and **b** (48^2) represent a vibrational progression of the lowest-frequency mode ν_{48} (A″) of *p*-EP (Figure S1). The weak peak **c** is due to the final state 27^2; the ν_{27} mode is the second lowest-frequency mode or the lowest-frequency mode of A′ symmetry (ν_{27} = 89 cm^{-1}, Figure S1). According to the energic information, there are several possibilities for the Feshbach resonance 5, i.e., $48'^1 46'^1/27'^2 26'^1$ with A′ symmetry or $48'^3 27'^3$ with A″ symmetry. It is possible that all three DBS levels may contribute to Feshbach resonance 5. The first two can explain the final states **a** and **c**, while the third combinational level can explain peak **b** as a result of the violation of the propensity rule.[35] The spectra in Figure 7b,c both involve a fundamental vibrational level overlapping with more complicated combinational levels, resulting in the enhanced 0_0^0 transition and other vibrational final states. In Figure 7b, the enhancement of the final states B (26^1), D (25^1), and F ($26^1 25^1$) in comparison with Figure 1 can all be attributed to excitation to the $27'^2 26'^1 25'^1$ DBS level overlapping with the $22'^1$ fundamental level. All three autodetachment channels violate the propensity rule. The tremendous enhancement of the weak final state C ($27^1 26^1$) in Figure 7c is due to excitation to the $27'^1 26'^1 24'^1$ DBS level. The overlapping $26'^2 25'^1$ DBS level produces the final state **f** (26^2) and the enhanced peak F ($26^1 25^1$).

The enhanced peaks D (25^1) and E (24^1) in Figure 7d are due to excitation to the $25'^1 24'^1$ DBS level. The appearance of peak **h** is due to excitation to the overlapping DBS level $43'^1 26'^1$ with a strong mode selectivity, where the 26′ quantum is strongly coupled to the dipole-bound electron for the final state **h** (43^1). The enhanced final states in Figure 7e can come from excitations to the overlapping $27'^{1}26'^{1}25'^{2}$ and $27'^{1}25'^{1}23'^{1}$ DBS levels with multiple autodetachment possibilities, if the violation of the propensity rule is considered. The enhanced peak F ($23^1/26^{1}25^{1}$, Table 1) can come from the $27'^{1}26'^{1}25'^{2}$ DBS level with the coupling of the $27'^{1}25'^{1}$ quanta to the dipole-bound electron to give the $26^{1}25^{1}$ final state or from the $27'^{1}25'^{1}23'^{1}$ DBS level by again coupling the $27'^{1}25'^{1}$ quanta to give the 23^1 final state. The enhanced final states **i** ($27^{1}23^{1}$) and **k** ($27^{1}25^{2}$) are produced from the two overlapping DBS levels each following the propensity rule. Figure 7f taken at Feshbach resonance 28 shows probably the most complicated resonant photoelectron spectrum with at least five enhanced vibrational final states involving four overlapping DBS levels. The dominating DBS level is $25'^{1}22'^{1}$, resulting in the enhanced final states D (25^1) and H (22^1). The enhanced final state F (23^1), **h** (43^1), and **l** (19^1) are due to autodetachment from the $48'^{2}24'^{1}23'^{1}$, $43'^{1}24'^{1}$, and $47'^{1}19'^{1}$ DBS levels, respectively. Finally, the resonant photoelectron spectrum taken at Feshbach resonance 32 in Figure 7g involves excitation to three DBS levels. The main excitation is to the $24'^{1}22'^{1}$ DBS level, yielding the enhanced E (24^1) and H (22^1) final states. The enhanced final states G ($26^{1}24^{1}$) and J ($25^{1}24^{1}$) are due to autodetachment from the $48'^{2}26'^{1}24'^{2}$ and $45'^{1}25'^{1}24'^{1}$ DBS levels, respectively.

The assignments of the final states of all the resonant and nonresonant photoelectron spectra of p-EP$^-$ are given in Table 1, and those of all the vibrational levels of the DBS from PDS are summarized in Table 2. The autodetachment processes from all the 32 Feshbach resonances are presented schematically in Figures 10 and 11.

4.6. Vibrational Information about the *p*-EP Radical

Combining the PDS and rPES, we are able to measure the fundamental frequencies of 17 vibrational modes for the p-EP radical, as summarized in Table 3. Vibrational frequencies are obtained for 11 modes with A′ symmetry and six modes with A″ symmetry for the p-EP radical. In particular, the frequencies for the two lowest-frequency modes, ν_{48} (A″) and ν_{27} (A’), are observed. In comparison, only six vibrational modes (ν_{22}−ν_{27} in Table 1) are observed in the nonresonant PES in Figure 1, all with A′ symmetry. The spectroscopic information obtained for such a complex and somewhat floppy system is unprecedented, proving once again the power of combining cryogenic cooling with photodetachment and resonant photoelectron spectroscopy involving an intermediate dipole-bound state for polar molecular radicals.

Table 3. Measured Vibrational Frequencies for the *p*-EP Radical from the Current Work Compared with the Theoretical Values at the B3LYP/aug-cc-pVTZ Level of Theory

vibrational mode	symmetry	experimental frequency (cm^{-1})[a]	theoretical frequency (cm^{-1})[b]
ν_{27}	A′	89(5)	89
ν_{26}		196(3)	200
ν_{25}		349(3)	348
ν_{24}		458(3)	456
ν_{23}		540(4)	537
ν_{22}		715(5)	710
ν_{21}		740(6)	745
ν_{19}		848(6)	849
ν_{18}		950(8)	937
ν_{15}		1053(5)	1040
ν_{14}		1146(5)	1141
ν_{48}	A″	34(6)	36
ν_{47}		212(8)	205
ν_{46}		333(7)	326
ν_{45}		365(8)	374
ν_{44}		447(12)	446
ν_{43}		609(6)	608

[a] Numbers in the parentheses indicate the experimental uncertainties in the last digit. The frequencies reported here are obtained by considering the data from both the photodetachment spectrum of the dipole-bound state and the resonant photoelectron spectra. [b] Scaling factor of 0.975 is applied.

5. CONCLUSION

In conclusion, we report a photodetachment spectroscopy and high-resolution photoelectron imaging study on cryogenically cooled *para*-ethylphenolate anions using our third-generation ESI-PES apparatus. The electron affinity of the *para*-ethylphenoxy radical was measured accurately to be 2.1604 ± 0.0004 eV (17425 ± 3 cm^{-1}). Photodetachment spectroscopy revealed a dipole-bound state with a binding energy of 145 ± 3 cm^{-1} and 33 vibrational levels of this DBS, including 32 Feshbach resonances. Resonant photoelectron spectra at the 32 Feshbach resonances were obtained, resulting in highly non-Franck-Condon vibrational distributions and allowing the observation of vibrational final states that are not accessible in conventional photoelectron spectroscopy. Intramolecular inelastic rescattering between the outgoing dipole-bound electron and the molecular core was observed to excite a low-frequency FC-inactive mode of p-EP in the resonant spectra. The combination of photodetachment spectroscopy and resonant photoelectron spectroscopy led to the measurement of frequencies for 17 vibrational modes of p-EP, including six symmetry-forbidden modes. The current study further confirmed the power of resonant photoelectron and photodetachment spectroscopy via DBSs, in combination with cryogenic cooling for obtaining rich vibrational information of complex molecular radicals.

■ ASSOCIATED CONTENT

Supporting Information

The Supporting Information is available free of charge at https://pubs.acs.org/doi/10.1021/prechem.2c00012.

> Computed vibrational frequencies of the normal modes for the p-EP neutral radical and the p-EP$^-$ anion; atomic displacement vectors of the normal modes for the p-EP neutral radical (PDF)

■ AUTHOR INFORMATION

Corresponding Author

Lai-Sheng Wang − *Department of Chemistry, Brown University, Providence, Rhode Island 02912, United States;* orcid.org/0000-0003-1816-5738; Email: Lai-Sheng_Wang@brown.edu

Authors

Dao-Fu Yuan – *Department of Chemistry, Brown University, Providence, Rhode Island 02912, United States;* orcid.org/0000-0001-8461-6889
Yue-Rou Zhang – *Department of Chemistry, Brown University, Providence, Rhode Island 02912, United States*
Chen-Hui Qian – *Department of Chemistry, Brown University, Providence, Rhode Island 02912, United States*
Guo-Zhu Zhu – *Department of Chemistry, Brown University, Providence, Rhode Island 02912, United States*

Complete contact information is available at: https://pubs.acs.org/10.1021/prechem.2c00012

Notes

The authors declare no competing financial interest.

■ ACKNOWLEDGMENTS

This work was supported by the Department of Energy, Office of Basic Energy Sciences, Chemical Sciences, Geosciences, and Biosciences Division under Grant DE-SC0018679. The calculation was performed using computational resources and services provided by CCV of Brown University.

■ REFERENCES

(1) Ho, J.; Ervin, K. M.; Lineberger, W. C. Photoelectron Spectroscopy of Metal Cluster Anions: Cu_n^-, Ag_n^-, and Au_n^-. *J. Chem. Phys.* **1990**, *93*, 6987–7002.

(2) Wang, L. S. Photoelectron Spectroscopy of Size-Selected Boron Clusters: From Planar Structures to Borophenes and Borospherenes. *Int. Rev. Phys. Chem.* **2016**, *35*, 69–142.

(3) Neumark, D. M. Slow Electron Velocity-Map Imaging of Negative Ions: Applications to Spectroscopy and Dynamics. *J. Phys. Chem. A* **2008**, *112*, 13287–13301.

(4) Wang, X. B.; Wang, L. S. Development of a Low-Temperature Photoelectron Spectroscopy Instrument Using an Electrospray Ion Source and a Cryogenically Controlled Ion Trap. *Rev. Sci. Instrum.* **2008**, *79*, 073108.

(5) Weichman, M. L.; Neumark, D. M. Slow Photoelectron Velocity-Map Imaging of Cryogenically Cooled Anions. *Annu. Rev. Phys. Chem.* **2018**, *69*, 101–124.

(6) Zhu, G. Z.; Wang, L. S. High-Resolution Photoelectron Imaging and Resonant Photoelectron Spectroscopy via Noncovalently Bound Excited States of Cryogenically Cooled Anions. *Chem. Sci.* **2019**, *10*, 9409–9423.

(7) Desfrancois, C.; Abdoul-Carime, H.; Schermann, J. P. Ground-State Dipole-Bound Anions. *Int. J. Mod. Phys. B* **1996**, *10*, 1339–1395.

(8) Compton, R. N.; Carman, H. S.; Desfrancois, C.; Abdoul-Carime, H.; Schermann, J. P.; Hendricks, J. H.; Lyapustina, S. A.; Bowen, K. H. On the Binding of Electrons to Nitromethane: Dipole and Valence Bound Anions. *J. Chem. Phys.* **1996**, *105*, 3472–3478.

(9) Compton, R. N.; Hammer, N. I. Multiple-Bound Molecular Anions. In *Advances in Gas-Phase Ion Chemistry*; Adams, N. G., Ed.; JAI: Greenwich, CT, 2001; Vol. *4*, pp 275–305.

(10) Jordan, K. D.; Wang, F. Theory of Dipole -Bound Anions. *Annu. Rev. Phys. Chem.* **2003**, *54*, 367–396.

(11) Jackson, R. L.; Zimmerman, A. H.; Brauman, J. I. Resonant States at Threshold Observed in Electron Photodetachment Cross Sections of Polyatomic Negative Ions. *J. Chem. Phys.* **1979**, *71*, 2088–2094.

(12) Lykke, K. R.; Mead, R. D.; Lineberger, W. C. Observation of Dipole-Bound States of Negative Ions. *Phys. Rev. Lett.* **1984**, *52*, 2221–2224.

(13) Mead, R. D.; Lykke, K. R.; Lineberger, W. C.; Marks, J.; Brauman, J. I. Spectroscopy and Dynamics of the Dipole-bound State of Acetaldehyde Enolate. *J. Chem. Phys.* **1984**, *81*, 4883–4892.

(14) Marks, J.; Comita, P. B.; Brauman, J. I. Threshold Resonances in Electron Photodetachment Spectra. Structural Evidence for Dipole-Supported States. *J. Am. Chem. Soc.* **1985**, *107*, 3718–3719.

(15) Andersen, T.; Lykke, K. R.; Neumark, D. M.; Lineberger, W. C. Autodetachment Study of the Electronic Spectroscopy of FeO^-. *J. Chem. Phys.* **1987**, *86*, 1858–1867.

(16) Yokoyama, K.; Leach, G. W.; Kim, J. B.; Lineberger, W. C.; Boldyrev, A. I.; Gutowski, M. Autodetachment Spectroscopy and Dynamics of Vibrationally Excited Dipole-bound States of H_2CCC^-. *J. Chem. Phys.* **1996**, *105*, 10706–10718.

(17) Dessent, C. E. H.; Kim, J.; Johnson, M. A. Photochemistry of Halide Ion–Molecule Clusters: Dipole-Bound Excited States and the Case for Asymmetric Solvation. *Acc. Chem. Res.* **1998**, *31*, 527–534.

(18) Dao, D. B.; Mabbs, R. The Effect of the Dipole Bound State on AgF^- Vibrationally Resolved Photodetachment Cross Sections and Photoelectron Angular Distributions. *J. Chem. Phys.* **2014**, *141*, 154304.

(19) Mascaritolo, K. J.; Gardner, A. M.; Heaven, M. C. Autodetachment Spectroscopy of the Aluminum Oxide Anion Dipole Bound State. *J. Chem. Phys.* **2015**, *143*, 114311.

(20) Lu, Y.; Tang, R.; Fu, X.; Liu, H. D.; Ning, C. Dipole-Bound and Valence Excited States of AuF Anions via Resonant Photoelectron Spectroscopy. *J. Chem. Phys.* **2021**, *154*, 074303.

(21) Desfrancois, C.; Abdoulcarime, H.; Khelifa, N.; Schermann, J. P. From 1/r to $1/r^2$ Potentials - Electron-Exchange between Rydberg Atoms and Polar-Molecules. *Phys. Rev. Lett.* **1994**, *73*, 2436–2439.

(22) Hammer, N. I.; Diri, K.; Jordan, K. D.; Desfrancois, C.; Compton, R. N. Dipole-Bound Anions of Carbonyl, Nitrile, and Sulfoxide Containing Molecules. *J. Chem. Phys.* **2003**, *119*, 3650–3660.

(23) Hammer, N. I.; Hinde, R. J.; Compton, R. N.; Diri, K.; Jordan, K. D.; Radisic, D.; Stokes, S. T.; Bowen, K. H. Dipole-Bound Anions of Highly Polar Molecules: Ethylene Carbonate and Vinylene Carbonate. *J. Chem. Phys.* **2004**, *120*, 685–690.

(24) Qian, C. H.; Zhu, G. Z.; Wang, L. S. Probing the Critical Dipole Moment to Support Excited Dipole-Bound States in Valence-Bound Anions. *J. Phys. Chem. Lett.* **2019**, *10*, 6472–6477.

(25) Berry, R. S. Ionization of Molecules at Low Energies. *J. Chem. Phys.* **1966**, *45*, 1228–1245.

(26) Simons, J. Propensity Rules for Vibration-Induced Electron Detachment of Anions. *J. Am. Chem. Soc.* **1981**, *103*, 3971–3976.

(27) Liu, H. T.; Ning, C. G.; Huang, D. L.; Dau, P. D.; Wang, L. S. Observation of Mode-Specific Vibrational Autodetachment from Dipole-Bound States of Cold Anions. *Angew. Chem. Int. Ed.* **2013**, *52*, 8976–8979.

(28) Huang, D. L.; Zhu, G. Z.; Wang, L. S. Observation of Dipole-Bound State and High-Resolution Photoelectron Imaging of Cold Acetate Anions. *J. Chem. Phys.* **2015**, *142*, 091103.

(29) Huang, D. L.; Liu, H. T.; Ning, C. G.; Wang, L. S. Vibrational State-Selective Autodetachment Photoelectron Spectroscopy from Dipole-Bound States of Cold 2-Hydroxyphenoxide: $o\text{-}HO(C_6H_4)O^-$. *J. Chem. Phys.* **2015**, *142*, 124309.

(30) Huang, D. L.; Liu, H. T.; Ning, C. G.; Zhu, G. Z.; Wang, L. S. Probing the Vibrational Spectroscopy of the Deprotonated Thymine Radical by Photodetachment and State-Selective Autodetachment Photoelectron Spectroscopy via Dipole-Bound States. *Chem. Sci.* **2015**, *6*, 3129–3138.

(31) Huang, D. L.; Ning, C. G.; Liu, H. T.; Wang, L. S. Conformation-Selective Resonant Photoelectron Spectroscopy via Dipole-Bound States of Cold Anions. *J. Phys. Chem. Lett.* **2015**, *6*, 2153–2157.

(32) Zhu, G. Z.; Huang, D. H.; Wang, L. S. Conformation-Selective Resonant Photoelectron Imaging from Dipole-Bound States of Cold 3-Hydroxyphenoxide. *J. Chem. Phys.* **2017**, *147*, 013910.

(33) Huang, D. L.; Zhu, G. Z.; Liu, Y.; Wang, L. S. Photodetachment Spectroscopy and Resonant Photoelectron Imaging of Cryogenically-Cooled Deprotonated 2-Hydroxypyrimidine Anions. *J. Mol. Spectrosc.* **2017**, *332*, 86–93.

(34) Zhu, G. Z.; Huang, D. H.; Wang, L. S. Conformation-Selective Resonant Photoelectron Imaging from Dipole-Bound States of Cold 3-Hydroxyphenoxide. *J. Chem. Phys.* **2017**, *147*, 013910.

(35) Huang, D. L.; Liu, H. T.; Ning, C. G.; Dau, P. D.; Wang, L. S. Resonant Photoelectron Imaging of Deprotonated Uracil Anion via Vibrational Levels of a Dipole-Bound Excited State. *Chem. Phys.* **2017**, *482*, 374−383.

(36) Zhu, G. Z.; Qian, C. H.; Wang, L. S. Dipole-Bound Excited States and Resonant Photoelectron Imaging of Phenoxide and Thiophenoxide Anions. *J. Chem. Phys.* **2018**, *149*, 164301.

(37) Zhu, G.-Z.; Qian, C.-H.; Wang, L.-S. Tautomer-Specific Resonant Photoelectron Imaging of Deprotonated Cytosine Anions. *Angew. Chem. Int. Ed.* **2019**, *58*, 7856−7860.

(38) Zhu, G. Z.; Cheung, L. F.; Liu, Y.; Qian, C. H.; Wang, L. S. Resonant Two-Photon Photoelectron Imaging and Intersystem Crossing from Excited Dipole-Bound States of Cold Anions. *J. Phys. Chem. Lett.* **2019**, *10*, 4339−4344.

(39) Qian, C.-H.; Zhu, G.-Z.; Zhang, Y.-R.; Wang, L.-S. Photodetachment Spectroscopy and Resonant Photoelectron Imaging of the 2-Naphthoxide Anion via Dipole-Bound Excited States. *J. Chem. Phys.* **2020**, *152*, 214307.

(40) Yuan, D. F.; Liu, Y.; Qian, C. H.; Zhang, Y. R.; Rubenstein, B. M.; Wang, L. S. Observation of a π-Type Dipole-Bound State in Molecular Anions. *Phys. Rev. Lett.* **2020**, *125*, 073003.

(41) Yuan, D. F.; Liu, Y.; Qian, C. H.; Kocheril, G. S.; Zhang, Y. R.; Rubenstein, B. M.; Wang, L. S. Polarization of Valence Orbitals by the Intramolecular Electric Field from a Diffuse Dipole-Bound Electron. *J. Phys. Chem. Lett.* **2020**, *11* (18), 7914−7919.

(42) Qian, C. H.; Zhang, Y. R.; Yuan, D. F.; Wang, L. S. Photodetachment Spectroscopy and Resonant Photoelectron Imaging of Cryogenically Cooled 1-Pyrenolate. *J. Chem. Phys.* **2021**, *154*, 094308.

(43) Yuan, D. F.; Zhang, Y. R.; Qian, C. H.; Liu, Y.; Wang, L. S. Probing the Dipole-Bound State in the 9-Phenanthrolate Anion by Photodetachment Spectroscopy, Resonant Two-Photon Photoelectron Imaging, and Resonant Photoelectron Spectroscopy. *J. Phys. Chem. A* **2021**, *125*, 2967−2976.

(44) Zhang, Y. R.; Yuan, D. F.; Qian, C. H.; Wang, L. S. Observation of A Dipole-Bound Excited State in 4-Ethynylphenoxide and Comparison with the Quadrupole-Bound Excited State in the Isoelectronic 4-Cyanophenoxide. *J. Chem. Phys.* **2021**, *155*, 124305.

(45) Yuan, D. F.; Zhang, Y. R.; Qian, C. H.; Wang, L. S. Resonant Two-Photon Photoelectron Imaging and Adiabatic Detachment Processes from Bound Vibrational Levels of Dipole-Bound States. *Phys. Chem. Chem. Phys.* **2022**, *24*, 1380−1389.

(46) Zhang, Y. R.; Yuan, D. F.; Wang, L. S. Probing the Strong Nonadiabatic Interactions in the Triazolyl Radical Using Photodetachment Spectroscopy and Resonant Photoelectron Imaging of Cryogenically-Cooled Anions. *J. Am. Chem. Soc.* **2022**, *144*, 16620−16630.

(47) Zhang, Y. R.; Yuan, D. F.; Wang, L. S. Observation of Core-Excited Dipole-Bound States. *J. Phys. Chem. Lett.* **2022**, *13*, 2124−2129.

(48) Yuan, D. F.; Zhang, Y. R.; Wang, L. S. Dipole-Bound State, Photodetachment Spectroscopy, and Resonant Photoelectron Imaging of Cryogenically-Cooled 2-Cyanopyrrolide. *J. Phys. Chem. A* **2022**, *126*, 6416−6428.

(49) Zhang, Y. R.; Yuan, D. F.; Wang, L. S. Investigation of the Electronic and Vibrational Structures of the 2-Furanyloxy Radical using Photoelectron Imaging and Photodetachment Spectroscopy via the Dipole-Bound State of the 2-Furanyloxide Anion. *J. Phys. Chem. Lett.* **2022**, *13*, 11481−11488.

(50) Wang, L. S. Electrospray Photoelectron Spectroscopy: From Multiply-Charged Anions to Ultracold Anions. *J. Chem. Phys.* **2015**, *143*, 040901.

(51) León, I.; Yang, Z.; Liu, H.-T.; Wang, L. S. The Design and Construction of a High-Resolution Velocity-Map Imaging Apparatus for Photoelectron Spectroscopy Studies of Size-Selected Clusters. *Rev. Sci. Instrum.* **2014**, *85*, 083106.

(52) Wang, L. S.; Ding, C. F.; Wang, X. B.; Barlow, S. E. Photodetachment Photoelectron Spectroscopy of Multiply Charged Anions Using Electrospray Ionization. *Rev. Sci. Instrum.* **1999**, *70*, 1957−1966.

(53) Tseng, C.-M.; Lee, Y. T.; Ni, C.-K.; Chang, J.-L. Photodissociation Dynamics of the Chromophores of the Amino Acid Tyrosine: *p*-Methylphenol, *p*-Ethylphenol, and *p*-(2-Aminoethyl) Phenol. *J. Phys. Chem. A* **2007**, *111*, 6674−6678.

(54) Castellani, M. E.; Anstöter, C. S.; Verlet, J. R. R. On the Stability of a Dipole-Bound State in the Presence of a Molecule. *Phys. Chem. Chem. Phys.* **2019**, *21*, 24286−24290.

(55) Garcia, G. A.; Nahon, L.; Powis, I. Two-Dimensional Charged Particle Image Inversion Using a Polar Basis Function Expansion. *Rev. Sci. Instrum.* **2004**, *75*, 4989−4996.

(56) Dribinski, V.; Ossadtchi, A.; Mandelshtam, V. A.; Reisler, H. Reconstruction of Abel-Transformable Images: The Gaussian Basis-Set Expansion Abel Transform Method. *Rev. Sci. Instrum.* **2002**, *73*, 2634−2642.

(57) Frisch, M. J.; Trucks, G. W.; Schlegel, H. B.; Scuseria, G. E.; Robb, M. A.; Cheeseman, J. R.; Scalmani, G.; Barone, V.; Mennucci, B.; Petersson, G. A.; et al. *Gaussian 09*, revision D.01; Gaussian, Inc.: Wallingford, CT, 2009.

(58) Liu, H. T.; Ning, C. G.; Huang, D. L.; Wang, L. S. Vibrational Spectroscopy of the Dehydrogenated Uracil Radical via Autodetachment of Dipole-Bound Excited States of Cold Anions. *Angew. Chem. Int. Ed.* **2014**, *53*, 2464−2468.

(59) Zhu, G. Z.; Liu, Y.; Wang, L. S. Observation of Excited Quadrupole-Bound States in Cold Anions. *Phys. Rev. Lett.* **2017**, *119*, 023002.

(60) Wigner, E. P. On the Behavior of Cross Sections Near Thresholds. *Phys. Rev.* **1948**, *73*, 1002−1009.

(61) Gunion, R. F.; Gilles, M. K.; Polak, M. L.; Lineberger, W. C. Ultraviolet Photoelectron Spectroscopy of the Phenide, Benzyl and Phenoxide Anions, with Ab initio Calculations. *Int. J. Mass Spectrom. Ion Processes* **1992**, *117*, 601−620.

(62) Kim, J. B.; Yacovitch, T. I.; Hock, C.; Neumark, D. M. Slow Photoelectron Velocity-Map Imaging Spectroscopy of the Phenoxide and Thiophenoxide Anions. *Phys. Chem. Chem. Phys.* **2011**, *13*, 17378−17383.

(63) Kang, D. H.; An, S.; Kim, S. K. Real-Time Autodetachment Dynamics of Vibrational Feshbach Resonances in a Dipole-Bound State. *Phys. Rev. Lett.* **2020**, *125*, 093001.

(64) Ciborowski, S. M.; Liu, G.; Graham, J. D.; Buytendyk, A. M.; Bowen, K. H. Dipole-Bound Anions: Formed by Rydberg Electron Transfer (RET) and Studied by Velocity Map Imaging-Anion Photoelectron Spectroscopy (VMI-aPES). *Eur. Phys. J. D* **2018**, *72*, 139.

(65) Kang, D. H.; Kim, J.; Eun, H. J.; Kim, S. K. State-Specific Chemical Dynamics of the Nonvalence Bound State of Molecular Anions. *Acc. Chem. Res.* **2022**, *55*, 3032−3042.